Fault Detection and Exclusion Using Solution Separation and Chi-Squared ARAIM

MATHIEU JOERGER, Member, IEEE
BORIS PERVAN, Member, IEEE
Illinois Institute of Technology
Chicago, IL, USA

This paper provides new integrity and continuity risk evaluation methods for fault detection and exclusion (FDE) using receiver autonomous integrity monitoring (RAIM). These methods are developed for both solution separation (SS) and Chi-squared RAIM: they capture the fact that exclusion enables continuity risk reduction in exchange for a higher integrity risk. The two approaches are implemented in an example advanced RAIM (ARAIM) application for worldwide vertical guidance of aircraft using multiconstellation Global Navigation Satellite Systems (GNSS).

Manuscript received August 7, 2014; revised May 25, 2015, October 2, 2015; released for publication October 4, 2015.

DOI. No. 10.1109/TAES.2015.140589.

Refereeing of this contribution was handled by J. Morton.

Authors' address: Illinois Institute of Technology, MMAE, 10 West 32nd Street, E1 Building - Room 243, Chicago, IL 60616-3793. Corresponding author is M. Joerger, E-mail: (joermat@iit.edu).

I. INTRODUCTION

This paper describes the derivation, analysis, and evaluation of two new fault detection and exclusion (FDE) methods using receiver autonomous integrity monitoring (RAIM) [1, 2]: the first method is based on solution separation (SS) RAIM [2–4], and the second one on chi-squared residual-based (χ^2) RAIM [5, 6]. The SS and χ^2 approaches are the two most widely implemented RAIM methods for fault detection. This paper provides complete integrity and continuity risk equations, which extend the use of SS and χ^2 RAIM from detection only to FDE.

Global Navigation Satellite System (GNSS) measurements are vulnerable to rare-event faults including satellite failures, which can potentially lead to major integrity threats for users. To mitigate their impact, fault-detection algorithms such as RAIM can be implemented. RAIM exploits redundant ranging signals to achieve self-contained fault detection at the user receiver [1, 2]. With the modernization of the United States' Global Positioning System (GPS), the full deployment of Russia's GLONASS, and the emergence of Europe's Galileo and of China's Beidou, the number of redundant ranging signals increases dramatically, which opens the possibility to fulfill stringent navigation integrity requirements using RAIM [7]. In particular, RAIM can help alleviate requirements on ground monitors. For example, researchers in the European Union and in the U.S. are investigating advanced RAIM (ARAIM) for worldwide vertical guidance of aircraft [8–10].

To further emphasize the impact of future multiconstellation GNSS on satellite redundancy, which is key to RAIM performance, Fig. 1 shows nominal space vehicle (SV) constellations for four GNSS. In this regard, it is worth reminding that using measurements from a single constellation, four satellites are required for positioning, five are needed for RAIM-based detection of single-SV faults, and six are needed for exclusion of single-SV faults [11]. In Fig. 1, signals received at an example location (Chicago, USA) are represented with thick black lines. Whereas each individual constellation only provides about five to ten ranging measurements, the joint constellation can provide continuous, global coverage of 25 to 35 satellites.

Two conflicting aspects of RAIM-based fault detection arise from the addition of new redundant ranging signals in multiconstellation GNSS. On the one hand, the integrity monitoring performance using ARAIM is improving [10]. On the other hand, the heightened likelihood of satellite faults because of the larger number of SVs causes more occurrences of mission interruptions due to faults being detected, thereby increasing the continuity risk.

In response, fault-exclusion algorithms have been designed and implemented in [9, 11, 12]. The word "exclusion" is employed to designate the choice of an estimator, which uses a subset of measurements rather than the full set [13]. Other terms in place of exclusion

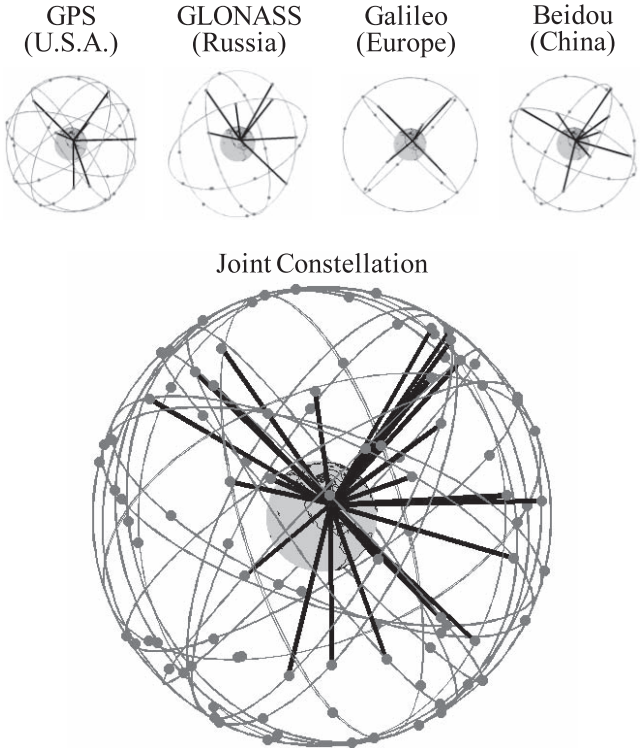

Fig. 1. Nominal satellite constellations for future GNSS. Signals received at example location (Chicago, USA) are represented by thick black lines.

have been used in the literature, including "isolation" [12], "identification" [14], and "reconfiguration" [11].

One of the primary motivations for implementing exclusion is to reduce continuity risk. (Another objective of fault exclusion can be to reduce the length of continuous unavailability periods, which is discussed in [15].) The interpretation of continuity risk requirements must therefore be clarified as it can vary, for example, depending on approach category in aircraft landing operations [16]. This paper takes a conservative interpretation of the continuity requirement, assuming that the detection function is not used before starting the approach, and that continuity is evaluated in a specific sense (for each approach) rather than in an averaged sense (over multiple approaches). A different interpretation can often be adopted, as is the case in ARAIM, which targets localizer performance with vertical guidance (LPV) requirements [9, 10, 17]. But, in this work, we derive continuity and integrity risk evaluation methods that are intended to be generally applicable, even under the more conservative approach-specific interpretation.

Under this assumption, one crucial element, which has been described as missing in [5] and [18], is a rigorous derivation of the integrity risk and continuity risk for RAIM FDE. Integrity risk evaluation is challenging because it involves quantifying the impact on state estimate errors of undetected faults and of wrong exclusions. A priori integrity and continuity risk evaluation is needed when designing navigation systems to meet specific requirements, and it is needed operationally to predict if a mission (e.g., an aircraft approach) can be safely initiated.

In order to avoid making assumptions on the unknown fault distribution, integrity risk evaluation can be carried out using either of two implementations: either by directly searching for the worst case fault through the threat space, or using an integrity risk bounding process to formulate compact-form, easy-to-compute protection levels (PLs) (which are probabilistic bounds on the position estimate errors). The direct search approach is computationally more expensive than using PLs, but can provide a tighter integrity risk bound [19] under assumptions on nominal measurement error probability distributions that are detailed in this work.

Section II of this paper describes the two baseline detection methods: SS RAIM [5, 6] and χ^2 RAIM [2–4]. The SS RAIM test statistics are derived in the position domain, which is well suited for PL derivation. In parallel, χ^2 RAIM is derived at the measurement level, and in this work, is implemented using a direct search method. A detailed comparison of SS and χ^2 RAIM, for detection only, can be found in [19].

In Section III, general integrity and continuity risk equations for detection and exclusion are derived, which are valid even under the conservative interpretation of an approach-specific continuity risk requirement. The continuity risk equation focuses on mission interruptions due to fault detection without the possibility to exclude, but other sources of loss of continuity such as unscheduled satellite outages are also included [20, 21]. The integrity and continuity equations express the fact that the reduction in continuity risk, achieved using exclusion, comes at the cost of a higher integrity risk. They are used as a common starting point to establish the SS and χ^2 RAIM FDE methods in Sections IV and V, respectively.

In Section IV, an integrity risk bound for SS RAIM FDE is derived, which enables computationally efficient risk evaluation. A continuity risk bound is also given, which provides the means to determine detection and exclusion thresholds ensuring that the overall continuity risk requirement is satisfied.

In addition, in Section V, a χ^2 RAIM FDE method is devised based on parity space representations of the χ^2 RAIM detection and exclusion test statistics. Parity space representations are instrumental because the parity vector, which can be used to derive both the SS and χ^2 test statistics [22, 23], is the simplest, most fundamental measure of fault detection capability [12]. The paper will show that in parity space, for single-satellite faults, the no-detection and exclusion regions for SS RAIM are polytopic and prismatic, respectively, whereas for χ^2 RAIM, they are hyperspherical and cylindrical, respectively.

Finally, in Section VI, a performance analysis is carried out to assess worldwide availability of ARAIM FDE for an example aircraft approach navigation application using GPS, Galileo, GLONASS, and Beidou satellite constellations. Availability maps are established

assuming a conservative interpretation of the continuity risk requirement. The new SS and χ^2 RAIM methods are implemented to quantify integrity and continuity using both fault detection and exclusion.

II. BACKGROUND ON FAULT DETECTION USING RAIM

In this section, the integrity and continuity risks are defined for fault detection only, followed by notations for the least-squares (LS) estimator. Then, the baseline detection test statistics for χ^2 RAIM and SS RAIM are derived, and represented in parity space for a canonical example. The content of this section is used in the remainder of the paper to analyze fault-exclusion methods.

A. Integrity and Continuity Risks for Fault Detection

The integrity risk criterion is defined in [24] as

$$\sum_{i=0}^{h} P\left(|\varepsilon_0| > \ell, |q| < T \,\middle|\, H_i\right) P_{Hi} \le I_{REQ} - P_{NM} \quad (1)$$

where

- ε_0 is the error on the estimated parameter of interest (called "state" of interest)
- ℓ is a specified alert limit that defines hazardous situations (e.g., specified in [20] for aircraft approach navigation)
- q is the detection test statistic (q is used here to represent both the χ^2 and the SS test statistics)
- T is the detection threshold
- H_i for $i = 0, ..., h$ is a set of mutually exclusive, jointly exhaustive hypotheses. H_0 is the fault-free hypothesis. The remaining h fault hypotheses correspond to faults on subset measurement "I" (including single-satellite and multisatellite faults)
- P_{Hi} is the prior probability of H_i occurrence
- I_{REQ} is the integrity risk requirement (also specified in [20] for example aviation applications).
- P_{NM} is the prior probability of very rarely occurring faults that need not be monitored against (such that $P_{NM} < I_{REQ}$). References [9] and [25] describe procedures to define the number h of fault hypotheses that must be monitored against, while conservatively accounting for the remaining fault combinations using P_{NM} in (1). The smaller h is, the lighter the computational load of evaluating the left hand side in (1) gets, but the larger P_{NM} becomes.

We call integrity risk, or probability of hazardous misleading information (HMI) P_{HMI}, the left hand side in (1). To be rigorous, this term is the integrity risk under the $h + 1$ cases that are being monitored. The complete integrity risk bound is $P_{HMI} + P_{NM}$. To simplify terminology and notations in the remainder of the paper, P_{HMI} is referred to as the integrity risk.

The detection threshold T is typically set based on an allocated continuity risk requirement allocation $C_{REQ,0}$ (e.g., also specified in [20] for aviation applications) to limit the probability of false alarms (i.e., alarms under H_0) [11]. For detection only, T can be defined as

$$P\left(q \ge T | H_0\right) P_{H_0} \le C_{REQ,0}. \quad (2)$$

In addition, let n and m, respectively, be the number of measurements and number of parameters to be estimated (i.e., the "states"). The $n \times 1$ measurement vector $\mathbf{z}_*$ is assumed normally distributed with covariance matrix $\mathbf{V}_*$. Vector $\mathbf{z}_*$ is premultiplied by $\mathbf{V}_*^{-1/2}$ to obtain the "normalized" measurement equation:

$$\mathbf{z} = \mathbf{H}\mathbf{x} + \mathbf{v} + \mathbf{f} \quad (3)$$

where

- $\mathbf{z} = \mathbf{V}_*^{-1/2}\mathbf{z}_*$ is the normalized measurement vector
- $\mathbf{H}$ is the $n \times m$ normalized observation matrix
- $\mathbf{x}$ is the $m \times 1$ state vector
- $\mathbf{f}$ is the $n \times 1$ normalized fault vector
- $\mathbf{v}$ is the $n \times 1$ normalized measurement noise vector composed of zero-mean, unit-variance independent and identically distributed (IID) random variables.

We use the notation:

$$\mathbf{v} \sim \mathrm{N}\left(\mathbf{0}_{n\times 1}, \mathbf{I}_n\right) \quad (4)$$

where

- $\mathbf{0}_{a\times b}$ is an $a \times b$ matrix of zeros (in this case, it is an $n \times 1$ vector of zeros)
- $\mathbf{I}_n$ is an $n \times n$ identity matrix

In order to avoid making assumptions on unknown fault distributions, a bound on the probability of HMI given H_i can be evaluated for the worst case $n \times 1$ fault vector $\bar{\mathbf{f}}_i$:

$$P\left(|\varepsilon_0| > \ell, |q| < T | H_i\right) \le P\left(|\varepsilon_0| > \ell, |q| < T \,\middle|\, \bar{\mathbf{f}}_i\right). \quad (5)$$

The worst case fault vector $\bar{\mathbf{f}}_i$, which maximizes the integrity risk given H_i, is derived in [19] for multi-SV faults: the worst case fault direction can be expressed analytically, and the worst case magnitude is found using a straightforward line search algorithm. Thus, vector $\bar{\mathbf{f}}_i$ can be interpreted as a vector of deterministic measurement biases. For the fault-free case ($i = 0$), we use the notation $\bar{\mathbf{f}}_0 = \mathbf{0}$. The χ^2 RAIM approach adopted in this work directly uses the bound on the right hand side in (5), whereas in SS RAIM, a looser bound (given in Section IV) is typically implemented, which does not require determination of $\bar{\mathbf{f}}_i$.

It is a known result that ε_0 and q (for both χ^2 and SS RAIM) are statistically independent (see for example [22]), so that the joint probability in (5) can be expressed as

$$\begin{aligned} &P\left(|\varepsilon_0| > \ell, |q| < T \,\middle|\, \bar{\mathbf{f}}_i\right) \\ &\quad = P\left(|\varepsilon_0| > \ell \,\middle|\, \bar{\mathbf{f}}_i\right) P\left(|q| < T \,\middle|\, \bar{\mathbf{f}}_i\right). \end{aligned} \quad (6)$$

B. Baseline LS Estimator Used in RAIM

This section defines the estimate error ε_0 obtained using an LS estimator. Let x be the state of interest, for example the vertical position coordinate, which is often of primary concern for aircraft approach navigation. Let $\boldsymbol{\alpha}$ be an $m \times 1$ vector used to extract x out of the full state vector:

$$\boldsymbol{\alpha}^T = \begin{bmatrix} \mathbf{0}^T_{m_A \times 1} & 1 & \mathbf{0}^T_{m_B \times 1} \end{bmatrix} \tag{7}$$

where, in the order in which states
are stacked in $\mathbf{x}$, m_A and m_B are the number of states, respectively, before and after state x. Assuming that $\mathbf{H}$ is full rank and that $n \geq m$, the LS estimate of x is defined as

$$\hat{x}_0 \equiv \mathbf{s}_0^T \mathbf{z} \tag{8}$$

where

$$\mathbf{s}_0^T \equiv \boldsymbol{\alpha}^T \mathbf{P}_0 \mathbf{H}^T, \text{ and } \mathbf{P}_0 \equiv \left(\mathbf{H}^T \mathbf{H}\right)^{-1}. \tag{9}$$

The LS estimate error appearing in (1) is given by

$$\varepsilon_0 \equiv \hat{x}_0 - x = \mathbf{s}_0^T (\mathbf{v} + \mathbf{f}) \tag{10}$$

$$\varepsilon_0 \sim \mathrm{N}\left(\mathbf{s}_0^T \mathbf{f}, \sigma_0^2 \equiv \boldsymbol{\alpha}^T \mathbf{P}_0 \boldsymbol{\alpha}\right). \tag{11}$$

C. χ^2 RAIM Detection Test Statistic

The χ^2 RAIM detection test statistic is derived from the $(n-m) \times 1$ parity vector $\mathbf{p}$, which lies in the $(n-m)$-dimensional parity space, or left null space of $\mathbf{H}$, and can be expressed as [3, 22]

$$\mathbf{p} \equiv \mathbf{Q}\mathbf{z} = \mathbf{Q}(\mathbf{v} + \mathbf{f}) \tag{12}$$

where the $(n-m) \times n$ parity matrix $\mathbf{Q}$ is defined as

$$\mathbf{Q}\mathbf{Q}^T = \mathbf{I}_{n-m} \quad \text{and} \quad \mathbf{Q}\mathbf{H} = \mathbf{0}_{(n-m)\times m}. \tag{13}$$

The χ^2 RAIM detection test statistic is the square of the norm of $\mathbf{p}$, and can be written as [3, 22]

$$q_\chi^2 \equiv \mathbf{p}^T \mathbf{p} = \mathbf{r}^T \mathbf{r} \tag{14}$$

where $\mathbf{r}$ is the LS residual vector defined as

$$\mathbf{r} \equiv \mathbf{R}\mathbf{z} \tag{15}$$

where $\mathbf{R} \equiv (\mathbf{I}_n - \mathbf{H}\mathbf{P}_0\mathbf{H}^T)$. q_χ^2 follows a noncentral chi-square distribution with $(n-m)$ degrees of freedom and noncentrality parameter λ_χ^2 given by [22]

$$\lambda_\chi^2 \equiv \mathbf{f}^T \mathbf{Q}^T \mathbf{Q} \mathbf{f}. \tag{16}$$

D. SS RAIM Detection Test Statistics

As an alternative to χ^2 RAIM, a second integrity monitoring method called SS RAIM [5, 6] is considered. Let n_i be the number of simultaneously faulted SVs under a given fault hypothesis H_i. Without loss of generality, it is assumed that under H_i, the faulty measurements are the first n_i elements of $\mathbf{z}$. The measurement equation (3) can be partitioned following the equation:

$$\begin{bmatrix} \mathbf{A}_i^T \mathbf{z} \\ \mathbf{B}_i^T \mathbf{z} \end{bmatrix} = \begin{bmatrix} \mathbf{A}_i^T \mathbf{H} \\ \mathbf{B}_i^T \mathbf{H} \end{bmatrix} \mathbf{x} + \begin{bmatrix} \mathbf{A}_i^T \mathbf{v} \\ \mathbf{B}_i^T \mathbf{v} \end{bmatrix} + \begin{bmatrix} \mathbf{A}_i^T \mathbf{f} \\ \mathbf{0}_{(n-n_i)\times 1} \end{bmatrix} \tag{17}$$

with

$$\mathbf{A}_i \equiv \begin{bmatrix} \mathbf{I}_{n_i} & \mathbf{0}_{n_i \times (n-n_i)} \end{bmatrix}^T \text{ and } \mathbf{B}_i \equiv \begin{bmatrix} \mathbf{0}_{(n-n_i)\times n_i} & \mathbf{I}_{n-n_i} \end{bmatrix}^T. \tag{18}$$

Equation (17) is employed to distinguish the full-set solution $\hat{x}_0$ in (8), obtained using all n measurements in $\mathbf{z}$, from the subset solution $\hat{x}_i$, derived using only the $(n-n_i)$ fault-free measurements $\mathbf{B}_i^T \mathbf{z}$ under H_i. Assuming that $n - n_i \geq m$ and that $\mathbf{B}_i^T \mathbf{H}$ is full rank, $\hat{x}_i$ is defined as

$$\hat{x}_i \equiv \mathbf{s}_i^T \mathbf{z}, \text{ for } i = 1, ..., h \tag{19}$$

where

$$\mathbf{s}_i^T \equiv \boldsymbol{\alpha}^T \mathbf{P}_i \mathbf{H}^T \mathbf{B}_i \mathbf{B}_i^T, \quad \text{and} \quad \mathbf{P}_i \equiv \left(\mathbf{H}^T \mathbf{B}_i \mathbf{B}_i^T \mathbf{H}\right)^{-1}. \tag{20}$$

It follows that, under H_i, the estimate error ε_i is given by

$$\varepsilon_i \equiv \mathbf{s}_i^T (\mathbf{v} + \mathbf{f}) = \mathbf{s}_i^T \mathbf{v} \sim \mathrm{N}\left(0, \sigma_i^2 \equiv \boldsymbol{\alpha}^T \mathbf{P}_i \boldsymbol{\alpha}\right). \tag{21}$$

The solution separations are defined as [1, 5]

$$\Delta_i \equiv \hat{x}_0 - \hat{x}_i = \varepsilon_0 - \varepsilon_i, \quad \text{for } i = 1, ..., h. \tag{22}$$

Δ_i can also be expressed as [5, 6]

$$\Delta_i = \mathbf{s}_{\Delta i}^T \mathbf{z} \quad \text{and} \quad \Delta_i \sim \mathrm{N}\left(\mathbf{s}_{\Delta i}^T \mathbf{f}, \sigma_{\Delta i}^2\right) \tag{23}$$

where

$$\mathbf{s}_{\Delta i} \equiv \mathbf{s}_0 - \mathbf{s}_i \quad \text{and} \quad \sigma_{\Delta i}^2 = \sigma_i^2 - \sigma_0^2. \tag{24}$$

(Proof of (24) can be found in [6] and [19].)

For single-measurement faults, i.e., for $n_i = 1$, Δ_i can be written in terms of the parity vector $\mathbf{p}$ as [14, 23]

$$\Delta_i / \sigma_{\Delta i} = \mathbf{u}_i^T \mathbf{p} \tag{25}$$

where

$$\mathbf{u}_i \equiv \mathbf{Q}\mathbf{A}_i \left(\mathbf{A}_i^T \mathbf{Q}^T \mathbf{Q} \mathbf{A}_i\right)^{-1/2} \quad \text{for } i = 1, ..., n \tag{26}$$

with

$$\mathbf{A}_i = \begin{bmatrix} \mathbf{0}_{1\times(i-1)} & 1 & \mathbf{0}_{1\times(n-i)} \end{bmatrix}^T, \tag{27}$$

i.e., $\mathbf{Q}\mathbf{A}_i$ is the ith column of $\mathbf{Q}$. Vector $\mathbf{u}_i$ is the unit direction vector of the ith "fault mode line," which is the line described in parity space by the mean of $\mathbf{p}$ as the magnitude of a fault on the ith measurement varies from $-\infty$ to $+\infty$. Parity space representations are introduced below. Equation (25) expresses the fact that the n solution separations (there are $h = n$ solution separations when $n_i = 1$) are projections of the parity vector on their corresponding fault mode lines.

E. Parity Space Representations for a Canonical Example

In this section, both χ^2 RAIM and SS RAIM are represented in parity space for a canonical example used in [22, 23]. Let us consider a scalar state x and a 3×1 measurement vector $\mathbf{z}$ that are expressed as

$$\mathbf{z} = \mathbf{H}x + \mathbf{v} + \mathbf{f} \tag{28}$$

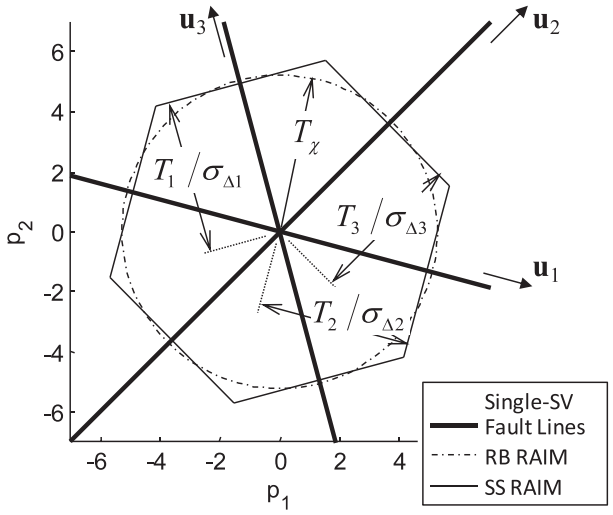

Fig. 2. Detection boundaries for χ^2 (circle) and SS (hexagon) in parity space. Detection is established if parity vector lands outside boundary.

where

$$\mathbf{H} = \begin{bmatrix} 1 & 1 & 1 \end{bmatrix}^T \quad \text{and} \quad \mathbf{v} \sim \mathrm{N}(\mathbf{0}_{3\times1}, \mathbf{I}_3). \tag{29}$$

Since $m = 1$ and $n = 3$, the $(n - m)$ parity space is two dimensional, which is convenient for display. The fault vector $\mathbf{f}$ represents three single-measurement faults with unknown fault magnitude f_i, for $i = 1, 2, 3$:

$$\mathbf{f} = \begin{bmatrix} f_1 & 0 & 0 \end{bmatrix}^T, \text{ or } \mathbf{f} = \begin{bmatrix} 0 & f_2 & 0 \end{bmatrix}^T, \text{ or } \mathbf{f} = \begin{bmatrix} 0 & 0 & f_3 \end{bmatrix}^T. \tag{30}$$

Their three fault mode lines, i.e., the lines described by the mean of $\mathbf{p}$ as f_i varies from $-\infty$ to $+\infty$, have direction vectors $\mathbf{u}_i$ defined in (26), and are represented in Fig. 2.

The detection boundaries for SS and χ^2 RAIM, respectively, are a polygon (or a polytope in higher dimensional parity space) and a circle (or a hypersphere). If the normalized SS thresholds are all the same ($T_1/\sigma_{\Delta1} = T_2/\sigma_{\Delta2} = T_3/\sigma_{\Delta3}$), then the polygon is a hexagon.

If the measurement vector $\mathbf{z}$ were noise free and fault free, the parity vector $\mathbf{p}$ would be the null vector. However, because of the combined effect of $\mathbf{v}$ and $\mathbf{f}$, $\mathbf{p}$ may land outside the detection boundary in Fig. 2, thereby establishing detection. Therefore, the probability of no detection is the probability of being inside the dash-dotted circle for χ^2 RAIM, and inside the hexagon for SS RAIM.

III. GENERAL INTEGRITY AND CONTINUITY RISK DEFINITIONS FOR FDE

This section defines general integrity and continuity risk equations for FDE, which are used as a common starting point to develop SS and χ^2 RAIM FDE methods in Sections IV and V.

Section II was limited to fault detection and did not address exclusion. For detection only, the probability of false alarms is limited by setting the detection thresholds to meet a continuity risk allocation $C_{REQ,0}$ as expressed in (2). However, the complete continuity risk accounts for all events causing mission interruptions. These events not only include cases of detection under fault-free conditions (i.e., false alarms), but also cases of detection under faulted conditions. Thus, the continuity risk equation for detection only is given by

$$P_{CONT} = P\left(D|H_0\right) P_{H0} + \sum_{i=1}^{h} P\left(D|H_i\right) P_{Hi} + P_{other} \tag{31}$$

where D is the detection event. The term P_{other} encompasses all other sources of loss of continuity, including the probability of unscheduled SV outages [20, 21]. When using a single constellation, P_{other} can represent a large portion of the continuity risk, but its contribution decreases in multiconstellation GNSS [15]. Since the focus of this paper is on exclusion, and since exclusion will not impact on P_{other}, performance evaluations will assume $P_{other} = 0$. P_{other} is included in the next equations for completeness.

It is worth noting that, in aviation applications that specify a lower severity level for events causing loss of continuity, P_{Hi} in (31) can be assumed lower than the state probability of fault used in the integrity risk equation (1). This is because for continuity, the requirement can sometimes be interpreted in an averaged sense, contrary to the integrity risk requirement, which is given in an approach-specific sense [15]. The details of this other interpretation are beyond the scope of this paper. In this work, the same conservative interpretation is applied to continuity and integrity, so that the same value of P_{Hi} is used in (1) and (31).

Under this interpretation, if the detector is efficient, then the second right hand side term in (31) is approximately equal to the prior probability of any fault occurring, i.e., $\sum_{i=1}^{h} P(D|H_i)P_{Hi} \approx \sum_{i=1}^{h} P_{Hi}$. If this probability is larger than the overall continuity risk requirement, noted C_{REQ}, which is likely to occur in multiconstellation GNSS, then faults need to be excluded to continue using the system. This is why fault-exclusion procedures were designed in [9, 11, 12]. However, this prior work does not provide the means to reliably predict the resulting integrity and continuity risks [5, 13].

FDE procedures can be described in three main steps:

1) The first step is the detection test described in Section II.
2) If a fault is detected, candidate subset measurements to be excluded are considered. A second set of tests, similar to the detection test, is carried out to ensure that the remaining nonexcluded measurements, which will be used for positioning, are fault free. An "exclusion test" is passed if no fault is detected in the remaining measurements.
3) Finally, if none of the exclusion tests are satisfied, the mission is interrupted, which impacts continuity. Conversely, if one or more candidate subsets meet

the exclusion test, then any one of these subsets can be excluded, which impacts integrity.

In this paper, the integrity risk bound for FDE is defined as

$$P_{HMI} \leq \sum_{i=0}^{h} P(HI_0, ND|H_i)P_{Hi} + \sum_{j=1}^{h}\sum_{i=0}^{h} P(HI_j, D, E_j|H_i)P_{Hi} \quad (32)$$

where

HI_j : hazardous information when using an LS estimator, defined in (8) for the full-set estimator $\mathbf{s}_0$, and in (20) for subset estimators $\mathbf{s}_j$, for, $j \neq 0$
ND : no detection,
E_j : exclusion test passed for subset j.

The first term in (32) is the same as the integrity risk given in (1) for detection only. The second term in (32) accounts for all fault hypotheses (subscript i) and all exclusion candidates (subscript j).

It is worth clarifying that the h fault hypotheses H_i are defined as mutually exclusive events in (1). For example, the following two hypotheses are mutually exclusive: 1) a fault affecting the first satellite only, and 2) a fault simultaneously affecting the first two satellites. In contrast, events E_j are not generally mutually exclusive: if the exclusion test is passed for removing the first satellite (e.g., if all but the first SV are fault free), then the test may also be satisfied for excluding the first two satellites.

In this regard, the sum over j in (32) provides an upper bound on the integrity risk, which accounts for the possibility of multiple exclusion tests being simultaneously satisfied. However, in practice, only one of the subsets verifying E_j is actually excluded. The choice of this subset is not imposed by (32). This approach is adopted because, in the event where more than one subset could be excluded, evaluating the risk of choosing one subset over another would be cumbersome. Instead, in this work, any candidate subset verifying E_j can be selected. Equation (32) remains bounding because P_{HMI} contributions under simultaneous E_j events are all added together, and this sum of probabilities is larger than the value of any individual term. Equality is obtained in (32) if events E_j, for $j = 1, ..., h$, compose a set of mutually exclusive events.

In parallel, the continuity risk is redefined to express that mission interruptions occur if a fault is detected, but cannot be excluded

$$P_{CONT} \equiv P(D, NE|H_0)P_{H0} + \sum_{i=1}^{h} P(D, NE|H_i)P_{Hi} + P_{other} \quad (33)$$

where NE is the "no exclusion" event, described in the third step of the above exclusion procedure. Equation (33) assumes that the exclusion function at the receiver has no impact on P_{other}, which is the case, for example, for SV outages.

Equations (32) and (33) capture a fundamental tradeoff of exclusion methods, which aim at reducing continuity risk at the expense of integrity risk. On the one hand, the continuity risk in (33) is lowered using exclusion as compared with using detection only in (31). The price to pay for this continuity risk reduction is expressed as the second term in (32), which is the integrity risk of performing an exclusion.

In Section IV and V, the above P_{HMI} and P_{CONT} definitions are implemented for SS RAIM and χ^2 RAIM.

IV. SS RAIM FDE

This section describes the SS RAIM FDE method. In Section IV-A, the three-step procedure outlined in Section III is applied to SS RAIM FDE. Then, in Section IV-B, integrity and continuity risk equations for SS FDE are derived. Finally, Section III-C provides parity space representations, which motivate the derivation of the new χ^2 RAIM FDE method in Section V.

A. Solution Separation FDE Exclusion Procedure

The following three-step SS RAIM FDE procedure is considered. First, the SS detection tests described in Section II are performed. A fault is detected if

$$|\Delta_k| \equiv \left|\hat{x}_0 - \hat{x}_k\right| \geq T_k \quad \text{for any } k, \quad k = 1, ..., h. \quad (34)$$

As expressed in (22), Δ_k can also be written as $\Delta_k = \varepsilon_0 - \varepsilon_k$.

Then, in case of detection, an attempt is made at exclusion. All exclusion candidate subsets "j," noted S_j, for $j = 1, ..., h$ are considered. Let $\hat{x}_j$ be the subset solution using the measurements remaining after exclusion of S_j, and let ε_j be the corresponding estimation error. In order to find $\hat{x}_j$ that can be assumed fault free, a second layer of detection is carried out using all subset solutions $\hat{x}_{j,l}$ within $\hat{x}_j$. Thus, S_j is excluded only if

$$|\Delta_{j,l}| \equiv \left|\hat{x}_j - \hat{x}_{j,l}\right| < T_{j,l} \quad \forall l, \begin{cases} l = 1, ..., h \\ \forall \mathrm{S}_l \not\subset \mathrm{S}_j \end{cases} \quad (35)$$

where $\hat{x}_{j,l}$ is the subset solution that excludes both subsets S_j and S_l. Equivalently, $\Delta_{j,l}$ can be expressed as $\Delta_{j,l} = \varepsilon_j - \varepsilon_{j,l}$, where $\varepsilon_{j,l}$ is the estimation error in $\hat{x}_{j,l}$. It is noteworthy that $|\Delta_{j,l}| \neq |\Delta_{l,j}|$.

Finally, if the exclusion test in (35) passes, then candidate solution $\hat{x}_j$ can be used for positioning and (32) provides a bound on the integrity risk. Conversely, if the exclusion test in (35) fails for all candidates $\hat{x}_j$ being tested (for $j = 1, ..., h$), then the mission is interrupted, which is the "NE"-event accounted for in (33).

Let τ_j be the number of SS exclusion tests needed to validate $\hat{x}_j$ in (35). τ_j is the total number of fault hypotheses h minus the number of hypotheses eliminated when excluding subset S_j. τ_j can be expressed as

$\tau_j = h - \sum_{k=1}^{n_j} C_k^{n_j}$, where n_j is the number of measurements in S_j, and C_k^n is the binomial coefficient. In addition, let τ be the total number of SS exclusion tests. Since τ_j exclusion tests are carried out for candidate subset S_j, for $j = 1, ..., h$, the number τ is given by $\tau = \sum_{j=1}^{h} \tau_j$. Thus, the total number of SS RAIM FDE tests is the sum of h detection tests and τ exclusion tests. Assuming single-SV faults (i.e., for $n_j = 1$), τ_j takes a much simpler expression: $\tau_j = h - 1$. In this case, the total number of SS tests is h^2, including h detection tests and $h(h-1)$ exclusion tests.

The integrity and continuity risk equations derived in Section IV-B for SS RAIM, and in Section V-A to V-C for χ^2 RAIM fully account for both single-SV and multi-SV faults. For clarity of explanation when discussing τ, and for graphical representation purposes in Sections IV-C and V-D, the single-SV fault case will be used as an example.

B. Integrity and Continuity Risk Bounds for SS FDE

Integrity risk evaluation using (32) is challenging because the estimation error and the detection and exclusion test statistics in the joint probabilities under the double-sum are correlated. In response, an upper bound for P_{HMI} is derived in Appendix A. The derivation is valid for estimators other than the LS estimator and is not restricted to single measurement faults. The resulting integrity risk bound is expressed as

$$\begin{aligned} P_{HMI} \le\ & P\left(|\varepsilon_0| > \ell \mid H_0\right) P_{H0} \\ & + \sum_{i=1}^{h} P\left(|\varepsilon_i| + T_i > \ell \mid H_i\right) P_{Hi} \\ & + \sum_{j=1}^{h} \left(\begin{array}{l} \sum\limits_{\substack{i=0 \\ S_i \subset S_j}}^{h} P\left(|\varepsilon_j| > \ell \mid H_i\right) P_{Hi} \\ + \sum\limits_{\substack{i=1 \\ S_i \subset S_j}}^{h} P\left(|\varepsilon_{j,i}| + T_{j,i} > \ell \mid H_i\right) P_{Hi} \end{array} \right) \end{aligned} \tag{36}$$

This bound is independent of the fault vector $\bar{\mathbf{f}}_i$ expressed in (5) and (6), which will not be the case in χ^2 RAIM.

The first two terms on the right hand side of (36) are a bound on the probability of hazardous information and no detection. A PL formulation equivalent to these two terms is typically used in SS RAIM for detection only [5, 6, 9]. Then, in (36), the sum over j accounts for all cases of hazardous information following detection, and exclusion. The first term within this sum is a bound on the probability of excluding a subset S_j that includes the faulted subset S_i ($S_i \subset S_j$). This term incorporates the fault-free hypothesis H_0, for which the notation S_0 designates an empty subset included in all S_j, for $j = 1, ..., h$. The second term under the j-indexed sum is a bound on the probability of wrong exclusion (defined as $S_i \not\subset S_j$) under faulty conditions. (This second term is a sum over τ_j terms, following the definition of τ_j in Section IV-A.)

The integrity risk bound in (36) is designed to enable risk evaluation in implementations where computational resources are limited. Appendix A identifies the key conservative assumptions required to obtain (36). In particular, the following two upper bounds are used in the derivation:

$$P(|\Delta_i| < T_i | H_i) = 1, \text{ and } P(|\Delta_{j,i}| < T_{j,i} | H_i) = 1. \tag{37}$$

These bounds are loose because in both cases, for large fault magnitudes, the probability of no-detection is much smaller than one. These key assumptions will later explain that our implementation of χ^2 RAIM provides a tighter integrity risk bound than SS RAIM.

In addition, in Appendix B, a bound on the continuity risk P_{CONT} is derived, which is expressed as

$$\begin{aligned} P_{CONT} \le & \sum_{i=1}^{h} P\left(|\Delta_i| \ge T_i \mid H_0\right) P_{H0} \\ & + \sum_{j=1}^{h} \sum_{\substack{i=1 \\ S_i \not\subset S_j}}^{h} P\left(|\Delta_{j,i}| \ge T_{j,i} \mid H_0\right) P_{Hi} + P_{other} \end{aligned} \tag{38}$$

This inequality provides the means to determine the h detection thresholds and the τ exclusion thresholds, while ensuring that the overall continuity risk requirement C_{REQ} is met.

The detection and exclusion thresholds can be written as

$$T_i = Q^{-1}\left\{\beta C_{REQ,i} / (2P_{H0})\right\} \sigma_{\Delta i} \tag{39}$$

$$T_{j,i} = Q^{-1}\left\{\alpha_j (1-\beta) C_{REQ,i} / 2P_{Hi}\right\} \sigma_{\Delta j,i} \tag{40}$$

where

$Q^{-1}\{\}$ is the inverse tail probability distribution of the two-tailed standard normal distribution (i.e., $Q\{\} = 1 - \Phi\{\}$, where $\Phi\{\}$ is the standard normal cumulative distribution function).

$\sigma^2_{\Delta j,i} = \sigma^2_{j,i} - \sigma^2_j$, and $\sigma_{j,i}$ is the standard deviation of the subset solution that excludes both S_i and S_j

and where the continuity risk allocation is performed in three steps. First, assuming $P_{other} < C_{REQ}$, a fraction $C_{REQ,i}$ of $C_{REQ} - P_{other}$, is allocated to each of the h fault hypotheses. $C_{REQ,i}$ is defined as

$$\begin{aligned} C_{REQ} - P_{other} &= \sum_{i=1}^{h} C_{REQ,i}, \text{ e.g.,} \\ C_{REQ,i} &= (C_{REQ} - P_{other})/h \end{aligned} \tag{41}$$

Then, under each fault hypothesis H_i, $C_{REQ,i}$ is allocated between the detection and the exclusion tests through parameter β, which is defined as

$$0 < \beta \le 1, \text{ e.g., } \beta = 1/2 \tag{42}$$

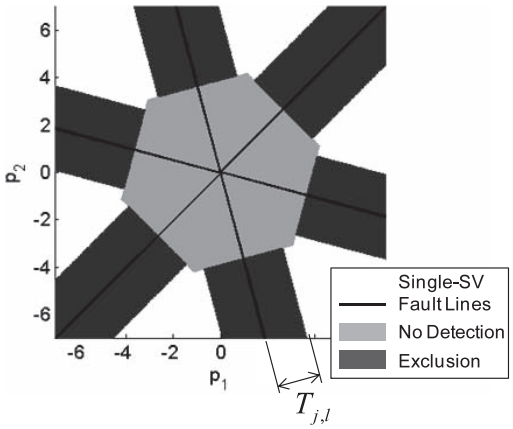

Fig. 3. No-detection and exclusion areas for SS RAIM in two-dimensional parity space. Measurement is excluded if parity vector lands in dark-shaded band surrounding measurement's fault line.

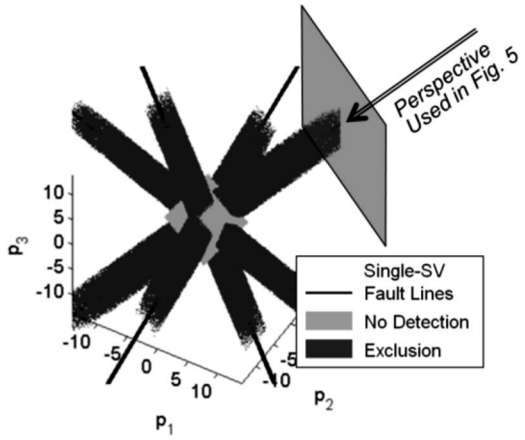

Fig. 4. No-detection and exclusion zones for SS RAIM in three-dimensional parity space.

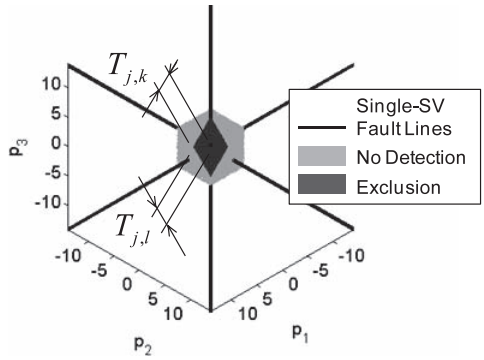

Fig. 5. Visualization of SS RAIM exclusion region. Multiple SS tests are required for each fault hypothesis to define exclusion regions.

An allocation of $\beta C_{REQ,i}$ is given for the detection test. Finally, the remaining continuity risk allocation of $(1-\beta)C_{REQ,i}$ is divided between the τ_i SS exclusion tests using parameters α_j defined as

$$\sum_{j=1}^{\tau_i} \alpha_j = 1, \text{ e.g., } \alpha_j = 1/\tau_i. \tag{43}$$

C. Parity Space Representation of SS RAIM FDE

This section assumes single-SV faults. The no-detection and exclusion regions can directly be represented in Fig. 3, for the canonical example described in Section II-E, by sampling the parity space and identifying points passing the detection and exclusion tests in (34) and (35). First, one can recognize the fair-gray, hexagonal SS-based no-detection area introduced earlier in Fig. 2. Then, Fig. 3 shows that the SS exclusion areas (dark gray) are bands surrounding the fault mode lines. These bands are sensible criteria for exclusion. If the parity vector is near a fault line, then it is easy to figure out which measurement to exclude. On the contrary, if the parity vector lands in between two fault mode lines, then it becomes extremely challenging to determine which of the two fault modes caused the error that was detected, and it may be safer not to exclude.

Fig. 3 displays disjoint exclusion regions (i.e., exclusion tests cannot be simultaneously satisfied for more than one candidate subset). But, it is worth reminding that the P_{HMI}-bounds in (32) and (36) do account for cases where exclusion regions overlap.

Exclusion regions can also be represented in higher dimensional parity space. For example, to obtain a three-dimensional parity space representation, the measurement vector $\mathbf{z}$ in (28) is augmented with one additional measurement, so that the observation matrix becomes $\mathbf{H} = [\,1\ 1\ 1\ 1\,]^T$. The 4×1 measurement noise vector $\mathbf{v}$ is still zero-mean normally distributed with covariance $\mathbf{I}_4$ and the 4×1 fault vector now includes one additional single-measurement fault mode.

The resulting no-detection and exclusion spaces are respectively shown in fair gray and dark gray in Fig. 4. Focusing on a single fault mode and looking at a plane normal to the corresponding fault mode line reveals the shape of the SS exclusion region, which is displayed in Fig. 5. For each fault hypothesis, SS RAIM uses $(h-1)$ test statistics to define an exclusion region. These SS test statistics are normally distributed, which is convenient for practical risk evaluation using PLs.

However, it can seem inefficient to use $(h-1)$ SS exclusion tests to describe a region surrounding a fault line. Instead, the number of tests can be reduced to one by defining a cylindrical exclusion region around the fault line. This is similar to the fact that the number of tests for detection only is h for SS RAIM versus one for χ^2 RAIM. This idea motivated the derivation of a χ^2 RAIM FDE method in Section V.

V. CHI-SQUARED RESIDUAL-BASED RAIM FDE

In this section, a new χ^2 RAIM FDE method is developed. First, Section V-A presents the derivation of new χ^2 RAIM exclusion test statistics, which are measures of the distance between the parity vector and the fault lines. The derivation deals with cases of multiple simultaneous SV faults. Then, Sections V-B and V-C

establish the χ^2 RAIM FDE integrity and continuity risk equations. Finally, in Section V-D, a parity space representation of this new method is provided.

A. Definition of the χ^2 RAIM Exclusion Test Statistic

Following the observation made at the end of Section IV, a χ^2 RAIM exclusion test statistic is derived, which provides a measure of the distance to the fault line. To achieve this, we determine the projection $\mathbf{q}_{\perp,j}$ of the parity vector $\mathbf{p}$ on the plane normal to the fault line with unit direction vector $\mathbf{u}_j$ under single-SV fault hypothesis H_j.

Let $q_{\perp,j}$ be the norm of $\mathbf{q}_{\perp,j}$ ($q^2_{\perp,j} \equiv \mathbf{q}^T_{\perp,j}\mathbf{q}_{\perp,j}$). Appendix C shows that, for single-SV and multi-SV fault hypotheses H_j, for $j = 1, ..., h$, $q_{\perp,j}$ is equivalent to the norm of the LS subset residual vector $\mathbf{r}_j$ ($\mathbf{r}_j \equiv \mathbf{R}_j\mathbf{z}$) obtained using all measurements except subset S_j. The exclusion test statistic $q^2_{\perp,j}$ can be expressed as

$$q^2_{\perp,j} = \mathbf{r}_j^T\mathbf{r}_j = \mathbf{z}^T\mathbf{R}_j\mathbf{z} \tag{44}$$

$$q^2_{\perp,j} \sim \chi^2\left(\mathbf{f}^T\mathbf{R}_j\mathbf{f}, n - m - n_j\right). \tag{45}$$

where

$$\mathbf{R}_j \equiv \mathbf{B}_j\mathbf{B}_j^T\left(\mathbf{I}_n - \mathbf{H}\left(\mathbf{H}^T\mathbf{B}_j\mathbf{B}_j^T\mathbf{H}\right)^{-1}\mathbf{H}^T\right)\mathbf{B}_j\mathbf{B}_j^T \tag{46}$$

(As a reminder, n_j is defined in (17) as the number of simultaneously faulted SVs under H_j, and the $(n - n_j) \times n$ matrix $\mathbf{B}_j^T$ is defined in (18) as a matrix of zeros and ones extracting the $(n - n_j)$ fault-free elements of $\mathbf{z}$.)

The χ^2 RAIM FDE procedure is identical to the SS approach described in Section IV-A, with the detection and exclusion test statistics q^2_χ and $q^2_{\perp,j}$ respectively replacing $|\Delta_k|$ and $|\Delta_{j,l}|$.

It follows that, using q^2_χ and $q^2_{\perp,j}$ instead of $|\Delta_k|$ and $|\Delta_{j,l}|$, the total number of detection and exclusion tests drops from $h + \tau$ for SS RAIM FDE to $h + 1$ for χ^2 RAIM FDE. For example, for single-SV faults, this number is reduced from h^2 using SS RAIM down to $h + 1$ using χ^2 RAIM (including one detection test and h exclusion tests for χ^2 RAIM).

B. Integrity Risk Bound for χ^2 RAIM FDE

A bound on the χ^2 RAIM FDE integrity risk is derived from the general P_{HMI} equation in (32). First, the following inequality is considered (same approach used for SS in Appendix A):

$$P(HI_j, D, E_j|H_i) \le P(HI_j, E_j|H_i) \tag{47}$$

Then, a worst case approach is implemented based on fault vectors $\bar{\mathbf{f}}_i$ and $\bar{\mathbf{f}}_{\perp,j,i}$, which respectively maximize the integrity risk in case of no-detection of a fault on subset S_i [same approach as in (5)], and in case of detection of a fault on S_i but exclusion of S_j. Assuming an LS estimator as in (6), the definitions of events HI_0, ND, HI_j, and E_j for χ^2 RAIM are used in (32) to directly express the P_{HMI}-bound as

$$P_{HMI} \le \sum_{i=0}^{h} P\left(|\varepsilon_0| > \ell \mid \bar{\mathbf{f}}_i\right) P\left(q^2_\chi < T^2_\chi \mid \bar{\mathbf{f}}_i\right) P_{Hi}$$
$$+ \sum_{j=1}^{h}\sum_{i=0}^{h} P\left(|\varepsilon_j| > \ell \mid \bar{\mathbf{f}}_{\perp,j,i}\right) P\left(q^2_{\perp,j} < T^2_{\perp,j} \mid \bar{\mathbf{f}}_{\perp,j,i}\right) P_{Hi} \tag{48}$$

For exclusion, the worst case direction of a fault impacting subset S_i is derived in the same manner as for detection [19], but using a set of measurements that excludes S_j. This worst case direction is expressed as

$$\bar{\mathbf{f}}_{\perp,j,i} = \mathbf{A}_i\left(\mathbf{A}_i^T\mathbf{R}_j\mathbf{A}_i\right)^{-1}\mathbf{A}_i^T\mathbf{s}_j, \tag{49}$$

In addition, (48) exploits the fact that ε_j and $q^2_{\perp,j}$ are statistically independent [for the exact same reason as ε_0 and q are independent in (6)]. Statistical independence between estimate error and test statistic is required to express the joint probabilities in (32) as products of probabilities in (48). This independence is only achievable using LS estimators [19], which places a constraint on the χ^2 RAIM estimator. The same constraint is not imposed on SS RAIM, which instead evaluates P_{HMI} using the bounding process described in Appendix A.

Finally, the χ^2 RAIM integrity risk bound in (48) does not require the conservative assumptions made in (36), so that χ^2 RAIM provides a tighter P_{HMI}-bound than SS RAIM. Also, (48) only uses $h + 1$ test statistics, versus h^2 for SS RAIM. However, in χ^2 RAIM, although the worst case fault direction is given by (49), the worst case fault magnitude still needs to be determined using a line-search algorithm. This search process ultimately causes χ^2 RAIM to be computationally more expensive than SS RAIM.

C. Continuity Risk Bound for χ^2 Residual-Based FDE

The χ^2 RAIM FDE continuity risk bound is derived in two steps, based on the general continuity risk definition in (33). First, the term of the sum corresponding to the fault-free hypothesis in (33) is rewritten as

$$\begin{aligned} &P\left(D, NE|H_0\right) \\ &\quad = P\left(q^2_\chi \ge T^2_\chi, q^2_{\perp,1} \ge T^2_{\perp,1}, ..., q^2_{\perp,h} \ge T^2_{\perp,h}|H_0\right) \\ &\quad \le P\left(q^2_\chi \ge T^2_\chi|H_0\right) \end{aligned} \tag{50}$$

Then, the remaining terms are addressed using the following inequality:

$$\begin{aligned} &P\left(D, NE|H_i\right) \\ &\quad = P\left(q^2_\chi \ge T^2_\chi, q^2_{\perp,1} \ge T^2_{\perp,1}, ..., q^2_{\perp,h} \ge T^2_{\perp,h}|H_i\right) \\ &\quad \le P\left(q^2_{\perp,i} \ge T^2_{\perp,i}|H_i\right) \\ &\quad \le P\left(q^2_{\perp,i} \ge T^2_{\perp,i}|H_0\right) \end{aligned} \tag{51}$$

The two upper bounds $P(q^2_{\perp,i} \ge T^2_{\perp,i}|H_i)$ and $P(q^2_{\perp,i} \ge T^2_{\perp,i}|H_0)$ are equivalent because, as expressed in

(44), the faulted measurement subset S_i is not included in the derivation of $q_{\perp,i}$ (i.e., $q_{\perp,i}$ is fault free under H_i).

Substituting (50) and (51) into (33), the χ^2 RAIM continuity risk bound can be expressed as

$$P_{CONT} \leq P(q_\chi^2 \geq T_\chi^2 | H_0) P_{H0} + \sum_{i=1}^{h} P(q_{\perp,i}^2 \geq T_{\perp,i}^2 | H_0) P_{Hi} + P_{other}. \quad (52)$$

The detection thresholds can therefore be written as

$$T_\chi^2 = \chi^{-2}\left\{1 - \beta(C_{REQ} - P_{other})/P_{H0}, n - m\right\} \quad (53)$$

$$T_{\perp,j}^2 = \chi^{-2}\left\{1 - (1-\beta)(C_{REQ} - P_{other})/P_{Hj}, n - m - n_j\right\} \quad (54)$$

where β is defined in (42) and $\chi^{-2}\{P, \delta\}$ is the inverse cumulative distribution function of the chi-square distribution with δ degrees of freedom at the probability value P. The continuity risk requirement allocations $C_{REQ,i}$ and parameters α_j defined in (41) and (43) for SS RAIM are not needed here since a single detection test and a single exclusion test per subset candidate are used in χ^2 RAIM.

The continuity risk requirement is allocated between $(h+1)$ test statistics for χ^2 RAIM, versus $(h+\tau)$ statistics for SS RAIM (i.e., assuming single-SV faults, $(h+1)$ χ^2 tests versus h^2 SS tests), which would suggest that the allocation can be more efficiently done using χ^2 RAIM. However, a detailed comparison in terms of continuity risk is beyond the scope of this paper, and is further discussed for detection only in [14, 24, 25].

D. Parity Space Representation of χ^2 RAIM FDE

This section presents parity space representations of χ^2 RAIM FDE. For the three- dimensional canonical example described in Section IV-C, Figs. 6 and 7 display the fair-gray spherical no-detection region at the origin, and the dark-gray cylindrical exclusion regions surrounding the faults lines. These regions are analogous to the SS RAIM polytopic and prismatic detection and exclusion regions shown in Figs. 4 and 5. Figs. 6 and 7 confirm that the χ^2 RAIM exclusion test statistic $q_{\perp,i}^2$ defined in (44) accomplishes the objective set at the beginning of this section of obtaining a cylindrical exclusion region using a single test statistic per fault hypothesis.

VI. Performance Evaluation

Sections IV and V have described two integrity and continuity risk evaluation methods for RAIM FDE. χ^2 RAIM enables direct integrity risk evaluation in (48) using $(h+1)$ detection and exclusion test statistics defined in (14) and (44), but requires that the worst case fault magnitudes for $\bar{\mathbf{f}}_i$ and $\bar{\mathbf{f}}_{\perp,j,i}$ be determined. In parallel, SS RAIM uses $(h+\tau)$ test statistics defined in (22) and (35) to provide a looser integrity risk bound given in (36),

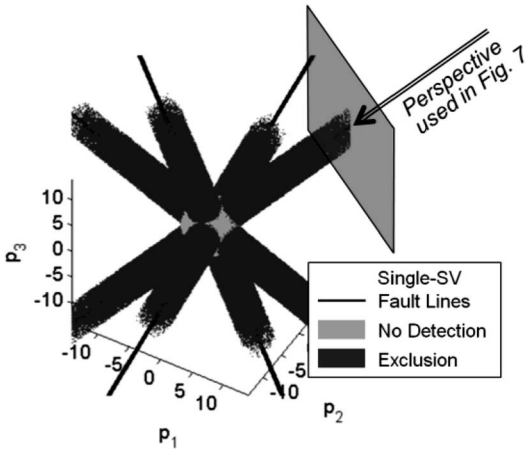

Fig. 6. No-detection and exclusion zones for χ^2 RAIM in three-dimensional parity space.

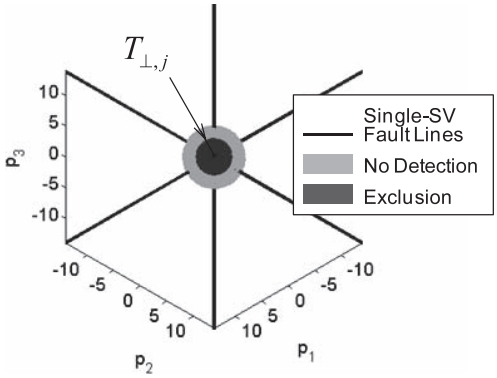

Fig. 7. Visualization of χ^2 RAIM exclusion region. In contrast with SS RAIM, single χ^2 test per fault hypothesis is sufficient to define exclusion regions.

which is independent of fault magnitudes, thereby enabling computationally efficient implementations.

This section aims at quantifying the integrity and continuity risks using SS and χ^2 RAIM, not only for fault detection, but also for fault exclusion.

A. Benchmark ARAIM Application, Requirements and Measurement Error Models

The SS and χ^2 RAIM methods derived in the previous sections are evaluated in an example ARAIM application for vertical guidance of aircraft using dual-frequency GPS, Galileo, GLONASS, and Beidou. Nominal satellite constellations used in this work comprise 24 GPS satellites [26], 24 Galileo satellites [27], 23 GLONASS satellites, and 27 Beidou satellites [28]. The simulation parameters, which include ARAIM measurement error models, and LPV-200 navigation requirements (to support localizer precision vertical aircraft approach operations down to 200 ft above the ground), are listed in Table I and described in detail in [9, 10]. Table I mentions that constellation-wide faults are not addressed in this paper. Constellation faults are faults that simultaneously impact all SVs in a same

TABLE I
Simulation Parameters

	Value			
Parameter	GPS	Galileo	GLO-NASS	Beidou
SV clock, orbit error,[b] URE [9]	0.5 m	0.67 m	0.8 m	0.8 m
SV clock, orbit error,[b] URA [9]	0.75 m	0.96 m	1 m	1 m
Residual tropo. error[a,b]		$0.12\frac{1.001}{(0.002001+\sin^2\xi)^{1/2}}$ m		
Smoothed code multipath[a,b]	$0.13+0.53e^{-\xi/10}$ m	lookup table [9]	same as GPS	same as GPS
Smoothed code receiver noise[a,b]	$0.15+0.43e^{-\xi/6.9}$ m	lookup table [9]	same as GPS	same as GPS
Fault-free range bias[c] b_{MAX}	0 m, or 0.75 m	0 m, or 1 m	0 m, or 1 m	0 m, or 1 m
I_{REQ}[d]		10^{-7}		
C_{REQ}[d]		$2{\cdot}10^{-6}$		
P_{Hi}[d]	10^{-5}	10^{-5}	10^{-5}	10^{-5}
P_{other}	0			
Constellation-wide faults		none considered		

[a] ξ is the satellite elevation angle in degrees
[b] standard deviation
[c] maximum value of mean error
[d] probability requirement

constellation [17]. For dual-GNSS ARAIM, exclusion is ineffective against such faults due to lack of constellation redundancy. In this case, other means of dealing with constellation faults must be considered [15, 29].

Also, ARAIM assumes two different error models, one "for continuity" and one "for integrity" (refer to [9] for details on implementing both error models). The standard deviations of the SV clock and orbit errors for the continuity and integrity models are, respectively, described in the first and second rows of Table I. The ARAIM error model for integrity assumes nonzero mean nominal measurement errors bounded by a bias b_{MAX} (even under fault-free conditions). Sections VI-B and VI-C first assume $b_{MAX}=0$ for consistency with (4). Nonzero nominal biases b_{MAX} are then addressed in Section VI-D.

The performance analysis will focus on the vertical position coordinate, for which the aircraft approach navigation requirements are often the most difficult to fulfill. Sensitivity to the vertical alert limit ℓ is evaluated for values ranging from 10 m to 35 m (LPV 200 requires $\ell=35$ m).

B. Integrity Risk Evaluation

In Fig. 8, the integrity risk P_{HMI} is evaluated over 24 h at an example Chicago location, for an example vertical alert limit $\ell=10$ m, for the joint GPS / Galileo system. P_{HMI}-bounds for χ^2 and SS RAIM FDE are, respectively, displayed with a thick, solid line and with a dotted line with black diamond markers. Despite a tight 10 m alert limit ℓ, the two curves are mostly below the 10^{-7} integrity risk requirement I_{REQ}, which is optimistic because, for now, the fault-free measurement bias b_{MAX} is assumed to be zero. The focus in Fig. 8 is on the comparison between the two proposed implementations of χ^2 and SS RAIM FDE. In this regard, χ^2 RAIM achieves P_{HMI}-values five to ten times lower than for SS RAIM. The fact that the χ^2 approach, based on a direct search for the worst case fault magnitude, provides a tighter integrity risk bound than SS RAIM is consistent with the theoretical analysis of Sections IV and V.

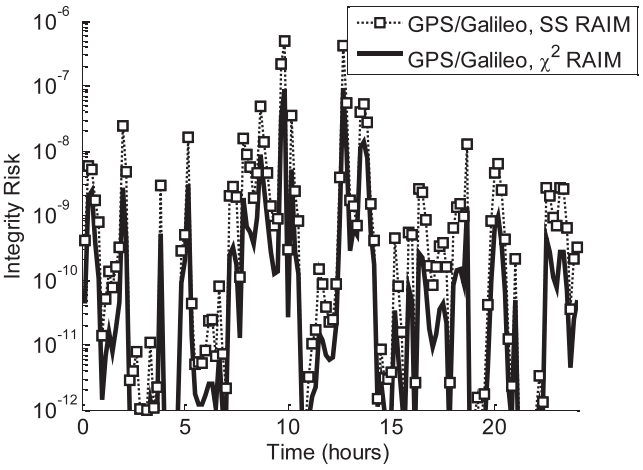

Fig. 8. Integrity risk evaluated using SS and χ^2 RAIM over 24 h at Chicago location, for $b_{MAX}=0$, for example alert limit of 10 m.

C. Worldwide Availability Evaluation

To further quantify the performance of χ^2 and SS RAIM FDE, availability maps are presented in Figs. 9 and 10 for an example 15 m alert limit ℓ, for a 10 deg $\times$ 10 deg latitude-longitude grid of locations, for GPS/Galileo satellite geometries simulated at regular 10 min intervals over a 24 h period. Availability is computed at each location as the fraction of time where the P_{HMI}-bound meets the integrity risk requirement I_{REQ}. In Figs. 9 and 10, availability is color-coded: white color corresponds to a value of 100%, black represents 98%. Constant availability contours are also shown for 99% and 100% probability levels. Fig. 9 displays darker areas than in Fig.

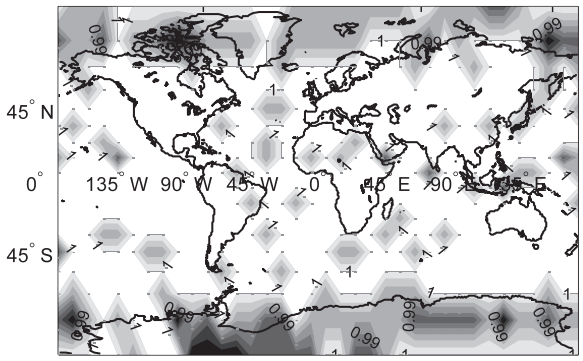

Fig. 9. Availability map for SS RAIM using GPS/Galileo, for b_{MAX}= 0, for alert limit of 15 m (coverage of 99.9% availability is 85.04%).

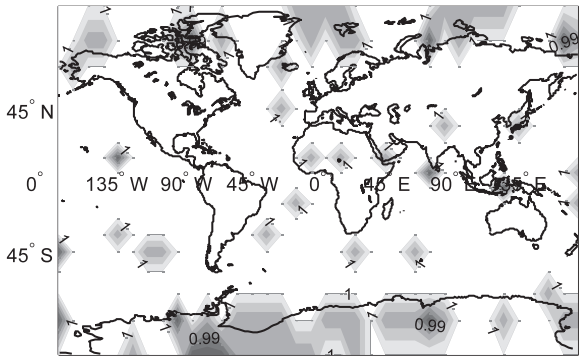

Fig. 10. Availability map for χ^2 RAIM using GPS/Galileo, for b_{MAX}= 0, for alert limit of 15 m (coverage of 99.9% availability is 93.44%).

10, which expresses again that lower availability is obtained using SS RAIM versus χ^2 RAIM.

In addition, the captions of Figs. 9 and 10 give a worldwide availability metric: the weighted coverage of 99.9% availability is defined as the percentage of grid point locations exceeding 99.9% availability; the coverage computation is weighted at each location by the cosine of the location's latitude, because grid point locations near the equator represent larger areas than near the poles. The figures show that the coverage of 99.9% availability increases from 85.04% for SS RAIM, to 93.44% for χ^2 RAIM, assuming $\ell = 15$ m.

D. Sensitivity of Coverage to Alert Limit

1) *Case of Nonzero Mean Nominal Measurement Errors*: In this section, the fault-free nominal biases are assumed unknown, but bounded by the nonzero values of b_{MAX} listed in Table I. For nonzero values of b_{MAX}, the assumption made in (4) is no longer satisfied. In response, Appendix D provides methods to evaluate the impact of b_{MAX} on P_{HMI} for SS and χ^2 RAIM FDE. In Appendix D, assumptions are made, which, contrary to Appendix A, are more conservative for χ^2 RAIM than for SS RAIM. It follows that, assuming $b_{MAX} > 0$, availability may or may not improve using χ^2 RAIM as compared with SS RAIM.

To illustrate this point, sensitivity of coverage to alert limit ℓ is evaluated in Fig. 11, for values of ℓ ranging from 10 m to 35 m. These preliminary results (not accounting

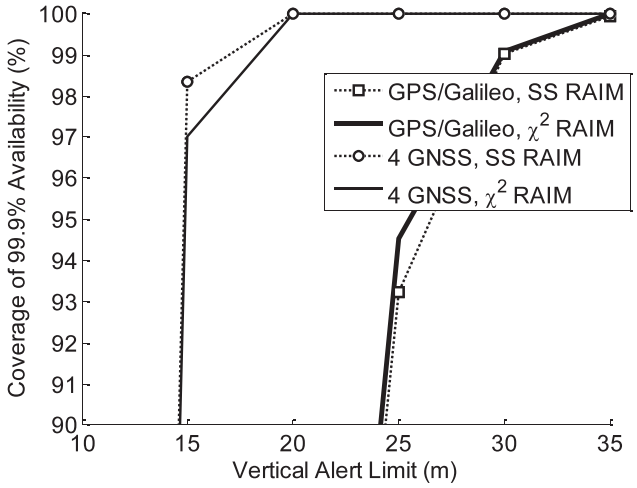

Fig. 11. Sensitivity of 99.9% availability coverage to alert limit, for $b_{MAX} > 0$, using SS RAIM versus using χ^2 RAIM.

for constellation faults, as mentioned in Table I) suggest that, using GPS/Galileo, the χ^2 RAIM availability curve (shown with a thick, solid line) is slightly above the SS RAIM curve (square markers), achieving 100% coverage for χ^2 RAIM for $\ell = 35$ m, versus 99.9% coverage for SS RAIM. In contrast, for the system using all four constellations (GPS, Galileo, GLONASS, and Beidou), the χ^2 RAIM availability curve (thin solid line) is below the SS curve (circular markers), but both methods reach 100% coverage for $\ell = 20$ m. In both cases (using two or four constellations), the processing time for χ^2 RAIM FDE was about 4.5 times longer than that of SS RAIM FDE. In this ARAIM application, for the parameter values given in Table I, the SS approach may be preferred.

The comparison between the proposed implementations of SS and χ^2 RAIM FDE can be summarized as follows. The χ^2 approach can provide tighter integrity risk bounds, and therefore higher availability, when assuming zero-mean nominal measurement errors ($b_{MAX} = 0$). This is because a direct search of the worst case fault is used in our implementation of χ^2 RAIM. On the other hand, this direct search makes χ^2 RAIM computationally more intensive than SS RAIM, which uses an efficient integrity risk bounding process. Additional complications arise in χ^2 RAIM when measurement errors are not zero mean ($b_{MAX} > 0$), which can cause the χ^2 approach to provide lower availability than SS RAIM (e.g., this is the case when using four GNSS in Fig. 11). Other implementations of SS and χ^2 RAIM FDE are possible (and will be investigated in future work), as for example, performing a direct search in SS RAIM, or deriving a different bound on the χ^2 RAIM FDE integrity risk.

VII. CONCLUSION

The emergence of multiconstellation GNSS opens a new era in navigation integrity monitoring, which may no longer require costly ground infrastructure, but instead may be performed at the user receiver using RAIM.

In this paper, two methods for FDE were considered, based on SS RAIM and on χ^2 RAIM. A new χ^2 RAIM exclusion test statistic was defined. It was shown that in parity space, for single-satellite faults, the SS RAIM no-detection and exclusion regions are polytopic and prismatic, respectively, whereas for χ^2 RAIM, they are hyperspherical and cylindrical, respectively. Integrity and continuity risk equations were then derived for both SS RAIM and χ^2 RAIM FDE, under hypotheses of single and multimeasurement faults. These equations mathematically express the tradeoff between continuity and integrity risk presented by the introduction of an exclusion function into RAIM.

A performance analysis was carried out for an example ARAIM application for worldwide vertical guidance of aircraft using measurements from GPS, Galileo, GLONASS, and Beidou satellites. Availability maps were established using methods that rigorously account for the integrity and continuity risk requirements, even when these are interpreted in a conservative, mission-specific sense. The new SS and χ^2 RAIM algorithms enable risk evaluation using both fault detection and exclusion.

APPENDIX A. INTEGRITY RISK BOUND FOR SS RAIM FDE

This Appendix provides a derivation of an integrity risk bound for SS RAIM FDE. In order to generate an SS integrity risk bound that is independent of fault magnitude, the general integrity risk equation (32) is rewritten to distinguish cases of: 1) no detection under fault-free conditions H_0, 2) no detection under faulty conditions H_i, 3) detection and exclusion of subset S_j that includes the faulted subset S_i, 4) detection and exclusion of S_j that does not include S_i:

$$\begin{aligned} P_{HMI} \le\ & P(HI_0,\, ND|H_0)P_{H0} \\ & + \sum_{i=1}^{h} P(HI_0,\, ND|H_i)P_{Hi} \\ & + \sum_{j=1}^{h} \left(\begin{array}{l} \sum\limits_{\substack{i=0 \\ S_i \subset S_j}}^{h} P(HI_j,\, D,\, E_j|H_i)P_{Hi} \\ + \sum\limits_{\substack{i=1 \\ S_i \not\subset S_j}}^{h} P(HI_j,\, D,\, E_j|H_i)P_{Hi} \end{array} \right) \end{aligned} \tag{55}$$

The following paragraphs provide upper bounds for each group of terms in (55).

For a set of events A_k, for $k = 1, ..., K$, we use the following notations:

$$\{A_k\ \forall k\} \equiv \left\{A_1, ..., A_K\right\} = \left\{A_1 \cap ... \cap A_K\right\}$$

$$\left\{(A_k)_{anyk}\right\} \equiv \left\{A_1 \cup ... \cup A_K\right\}.$$

Whenever it is appropriate to keep the same notations, subscripts i, j, and k, respectively, designate indices of fault hypotheses, exclusion hypotheses, and detection test statistics.

The first and second terms in (55) can be bounded using the following inequalities:

$$\begin{aligned} & P(HI,\, ND|H_0) \\ & \quad = P\left(|\varepsilon_0| > \ell,\, |\Delta_k| < T_k\ \forall k \,\middle|\, H_0\right) \\ & \quad \le P\left(|\varepsilon_0| > \ell \,\middle|\, H_0\right) \end{aligned} \tag{56}$$

$$\begin{aligned} & P(HI,\, ND|H_i) \\ & \quad = P\left(|\varepsilon_0| > \ell,\, |\Delta_k| < T_k\ \forall k \,\middle|\, H_i\right) \\ & \quad \le P\left(|\varepsilon_0| > \ell,\, |\Delta_i| < T_i \,\middle|\, H_i\right) \\ & \quad \le P\left(|\varepsilon_0| > \ell \,\middle|\, H_i,\, |\Delta_i| < T_i\right) P\left(|\Delta_i| < T_i \,\middle|\, H_i\right) \\ & \quad \le P\left(|\varepsilon_0| > \ell \,\middle|\, H_i,\, |\Delta_i| < T_i\right) \end{aligned} \tag{57}$$

Equations (56) and (57) are integrity risk bounds corresponding to PLs typically used in SS RAIM for detection only [5, 6, 9]. The last inequality in (57) uses the bound:

$$P(|\Delta_i| < T_i|H_i) = 1 \tag{58}$$

which is a loose bound: the probability of no detection under fault hypothesis H_i decreases as the fault magnitude increases. The bound in (58) causes the integrity risk bound to be larger for SS RAIM than for χ^2 RAIM. This bound was identified in [14] as a key difference between SS and χ^2 RAIM integrity risk bounds for detection only.

In addition, it is worth noting that no assumption needs be made in (57) on the correlation between ε_0 and Δ_i, so that these equations hold for estimators other than the LS estimator (ε_0 and Δ_i are only independent when using an LS estimator [19]). This will not be the case for χ^2 RAIM, which requires LS estimators to enable integrity risk evaluation using (48).

Then, the first term under the j-indexed sum in (55) accounts for the probability of hazardous information when excluding a subset S_j that includes the faulted subset S_i. This probability is upper-bounded using the following inequality:

$$\begin{aligned} & P(HI_j,\, D,\, E_j|H_i) \\ & = P\left(|\varepsilon_j| > \ell,\, |\Delta_k|_{anyk} \ge T_k,\, |\Delta_{j,l}| < T_{j,l}\ \forall S_l \not\subset S_j \,\middle|\, H_i\right) \\ & \le P\left(|\varepsilon_j| > \ell \,\middle|\, H_i\right) = P\left(|\varepsilon_j| > \ell \,\middle|\, H_0\right) \end{aligned} \tag{59}$$

In the first equation, event E_j is a joint-event of all τ_j SS exclusion tests $|\Delta_{j,l}| < T_{j,l}$ being simultaneously satisfied, for all subsets S_l that are not included in S_j (by definition of $\Delta_{j,l}$ in (35), if S_l is included in S_j, then $\Delta_{j,l}$ is not defined – or $\Delta_{j,l}$ would be zero). The last equation in (59) conditioned on H_0 instead of H_i expresses the fact that ε_j is fault free: the faulted subset S_i is excluded as part of S_j. Therefore, the distribution of ε_j is known.

The second sum of terms under the j-indexed sum in (55) deals with cases of wrong exclusions, also noted

WE_j, where the excluded subset S_j does not entirely eliminate the faulted subset S_i ($S_i \not\subset S_j$), and is upper-bounded using the following inequality:

$$\begin{aligned}
&P(HI_j, D, WE_j|H_i)\\
&= P\left(\begin{array}{l}|\varepsilon_j| > \ell, |\Delta_k|_{any\,k} \geq T_k,\\ |\Delta_{j,l}| < T_{j,l}\,\forall S_l \not\subset S_j \mid H_i\end{array}\right)\\
&\leq P\left(|\varepsilon_j| > \ell, |\Delta_{j,i}| < T_{j,i} \mid H_i\right)\\
&\leq P\left(|\varepsilon_j| > \ell \mid H_i, |\Delta_{j,i}| < T_{j,i}\right) P\left(|\Delta_{j,i}| < T_{j,i} \mid H_i\right)\\
&\leq P\left(|\varepsilon_j| > \ell \mid H_i, |\Delta_{j,i}| < T_{j,i}\right) \qquad (60)
\end{aligned}$$

In the last step of (60), the distribution of ε_j under H_i is biased by an unknown quantity because of the fault. The next paragraph shows that the condition on $\Delta_{j,i}$ sets a limit on the mean of ε_j. It is also worth noting that, similar to (58), the assumption that $P(|\Delta_{j,i}| < T_{j,i}|H_i) = 1$ generates a loose bound because, for large fault magnitudes, the probability of not detecting a fault in S_i using $\Delta_{j,i}$ is significantly smaller than one.

Finally, consider the following inequalities:

$$|\varepsilon_0| \leq |\varepsilon_i| + |\varepsilon_0 - \varepsilon_i| = |\varepsilon_i| + |\Delta_i| \qquad (61)$$

$$|\varepsilon_j| \leq |\varepsilon_{j,i}| + |\varepsilon_j - \varepsilon_{j,i}| = |\varepsilon_{j,i}| + |\Delta_{j,i}|. \qquad (62)$$

Substituting (61) into (57) and (62) into (60), making use of the conditions on $|\Delta_i|$ and $|\Delta_{j,i}|$ in (57) and (60), respectively, and substituting the resulting bounds together with (56) and (59) into (55), we obtain (36).

APPENDIX B. CONTINUITY RISK EQUATION FOR SS RAIM FDE

This Appendix provides a derivation of a continuity risk bound for SS RAIM FDE. First, the general continuity risk (33) is broken down to distinguish cases of no-exclusion under fault-free and under fault hypotheses:

$$\begin{aligned}
P_{CONT} = {} & P\left(D, NE|H_0\right) P_{H0}\\
& + \sum_{i=1}^{h} P\left(D, NE|H_i\right) P_{Hi} + P_{other}. \qquad (63)
\end{aligned}$$

The same notations as in Appendix A are used.

The first term in (63) can be bounded using the following inequality:

$$\begin{aligned}
&P\left(D, NE|H_0\right)\\
&= P\left(|\Delta_k|_{any\,k} \geq T_k, |\Delta_{j,l}|_{any\,l\neq j} \geq T_{j,l}\ \forall j \mid H_0\right)\\
&\leq P\left(|\Delta_k|_{any\,k} \geq T_k \mid H_0\right)\\
&\leq \sum_{k=1}^{h} P\left(|\Delta_k| \geq T_k \mid H_0\right) \qquad (64)
\end{aligned}$$

This bound is similar to the one typically used in SS for detection only to limit the probability of false alarms (a detailed explanation on the last inequality can be found in [14]).

The second term in (63) can be bounded in the following manner:

$$\begin{aligned}
&P\left(D, NE|H_i\right)\\
&= P\left(|\Delta_k|_{any\,k} \geq T_k, |\Delta_{j,l}|_{any\,l\neq j} \geq T_{j,l}\ \forall j \mid H_i\right)\\
&\leq P\left(|\Delta_{i,l}|_{any\,l\neq i} \geq T_{i,l} \mid H_i\right)\\
&= P\left(|\Delta_{i,l}|_{any\,l\neq i} \geq T_{i,l} \mid H_0\right)\\
&\leq \sum_{\substack{j=1\\ j\neq i}}^{h} P\left(|\Delta_{i,j}| \geq T_{i,j} \mid H_0\right) \qquad (65)
\end{aligned}$$

The probabilities in the final sum in (65) are conditioned upon H_0 although the initial term is conditioned upon H_i. This is essential because the test statistic distribution is known under H_0. This was achieved by isolating $|\Delta_{i,l}|$, defined in (35), which fully excludes faulty measurements S_i under H_i.

Finally, substituting (64) and (65) into (63) provides the continuity risk bound in (38).

APPENDIX C. TWO EQUIVALENT EXPRESSIONS OF THE CHI-SQUARED RAIM EXCLUSION TEST STATISTIC

This Appendix aims at proving that the exclusion test statistic $q_{\perp,j}$ can be evaluated as the distance of $\mathbf{p}$ to the jth fault line in parity space, or equivalently, as the norm of the LS subset measurement residual (excluding subset S_j).

The first paragraph of Section V-A explains that the χ^2 RAIM exclusion test statistic can be derived from the projection $\mathbf{q}_{\perp,j}$ of the parity vector $\mathbf{p}$ on the plane normal to the fault line with unit direction vector $\mathbf{u}_j$ under single-SV fault hypothesis H_j.

For multi-SV faults, graphical representations are not as useful as for single-SV faults. But, the mathematical derivation is identical, starting with the definition of $\mathbf{u}_j$ in (26), which can directly be applied to multi-SV faults to define an $(n-m)\times n_j$ matrix $\mathbf{U}_j$ as

$$\mathbf{U}_j \equiv \mathbf{Q}\mathbf{A}_j \left(\mathbf{A}_j^T\mathbf{Q}^T\mathbf{Q}\mathbf{A}_j\right)^{-1/2}. \qquad (66)$$

$\mathbf{U}_j$ provides the means to determine projections of $\mathbf{p}$ for multi-SV faults. The projected vector is expressed as

$$\mathbf{q}_{\perp,j} \equiv \left[\mathbf{I}_{n-m} - \mathbf{U}_j\mathbf{U}_j^T\right]\mathbf{p} \qquad (67)$$

where the $(n-m)\times(n-m)$ matrix $[\mathbf{I}_{n-m} - \mathbf{U}_j\mathbf{U}_j^T]$ is an orthogonal projection operator [30].

The χ^2 RAIM exclusion test statistic, defined as $q_{\perp,j}^2 \equiv \mathbf{q}_{\perp,j}^T\mathbf{q}_{\perp,j}$, can be written as

$$\begin{aligned}
q_{\perp,j}^2 &= \mathbf{z}^T\mathbf{Q}^T\left[\mathbf{I}_{n-m} - \mathbf{U}_j\mathbf{U}_j^T\right]^T\left[\mathbf{I}_{n-m} - \mathbf{U}_j\mathbf{U}_j^T\right]\mathbf{Q}\mathbf{z}\\
&= \mathbf{z}^T\mathbf{R}\mathbf{z} - \mathbf{z}^T\mathbf{R}^T\mathbf{A}_j\left(\mathbf{A}_j^T\mathbf{R}\mathbf{A}_j\right)^{-1}\mathbf{A}_j^T\mathbf{R}\mathbf{z}\\
&= \mathbf{z}^T\mathbf{R}^T\left[\mathbf{I} - \mathbf{A}_j\left(\mathbf{A}_j^T\mathbf{R}\mathbf{A}_j\right)^{-1}\mathbf{A}_j^T\right]\mathbf{R}\mathbf{z} \qquad (68)
\end{aligned}$$

where we used the facts that $\mathbf{Q}^T\mathbf{Q} = \mathbf{R}$ [22], and that matrix $\mathbf{U}_j\mathbf{U}_j^T$ is symmetric and idempotent. We use the notation:

$$\mathbf{T}_j \equiv \mathbf{R}^T\left[\mathbf{I}_n - \mathbf{A}_j\left(\mathbf{A}_j^T\mathbf{R}\mathbf{A}_j\right)^{-1}\mathbf{A}_j^T\right]\mathbf{R}. \tag{69}$$

The rest of the derivation aims at proving that $\mathbf{T}_j$ is equivalent to $\mathbf{R}_j$ in (46). This will accomplish the goal stated in the first sentence of this Appendix.

Let us define the symmetric idempotent matrices $\mathbf{X}$ and $\mathbf{Y}$ of dimensions $n_j \times n_j$ and $n \times n$, respectively, as

$$\mathbf{X} \equiv (\mathbf{A}_j^T\mathbf{R}\mathbf{A}_j)^{-1},\ \mathbf{Y} \equiv \mathbf{H}\mathbf{P}_0\mathbf{H}^T,\ \text{hence } \mathbf{R} = \mathbf{I}_n - \mathbf{Y} \tag{70}$$

Substituting $\mathbf{R}$ into (69) and expanding, $\mathbf{T}_j$ becomes

$$\begin{aligned}\mathbf{T}_j = \mathbf{I}_n - \mathbf{Y} - \mathbf{Y}\mathbf{A}_j\mathbf{X}\mathbf{A}_j^T\mathbf{Y}\\ -\mathbf{A}_j\mathbf{X}\mathbf{A}_j^T + \mathbf{A}_j\mathbf{X}\mathbf{A}_j^T\mathbf{Y} + \mathbf{Y}\mathbf{A}_j\mathbf{X}\mathbf{A}_j^T\end{aligned} \tag{71}$$

In parallel, premultiplying and postmultiplying $\mathbf{T}_j$ by $\mathbf{I}_n = \mathbf{A}_j\mathbf{A}_j^T + \mathbf{B}_j\mathbf{B}_j^T$, the following equation can be written:

$$\begin{aligned}\mathbf{T}_j = \mathbf{B}_j\mathbf{B}_j^T\mathbf{T}_j\mathbf{B}_j\mathbf{B}_j^T + \mathbf{A}_j\mathbf{A}_j^T\mathbf{T}_j\mathbf{B}_j\mathbf{B}_j^T\\ +\mathbf{B}_j\mathbf{B}_j^T\mathbf{T}_j\mathbf{A}_j\mathbf{A}_j^T + \mathbf{A}_j\mathbf{A}_j^T\mathbf{T}_j\mathbf{A}_j\mathbf{A}_j^T\end{aligned} \tag{72}$$

Substituting (71) into (72), and using the fact that

$$\mathbf{B}_j^T\mathbf{A}_j = \mathbf{0}_{(n-n_j)\times n_j} \quad \text{and} \quad \mathbf{A}_j^T\mathbf{B}_j = \mathbf{0}_{n_j\times(n-n_j)}, \tag{73}$$

the four terms in (72) simplify considerably. First, Substituting $\mathbf{B}_j\mathbf{B}_j^T = \mathbf{I}_n - \mathbf{A}_j\mathbf{A}_j^T$ into (46), using the matrix inversion lemma, and rearranging terms, $\mathbf{R}_j$ becomes

$$\mathbf{R}_j = \mathbf{B}_j\mathbf{B}_j^T\left(\mathbf{I}_n - \mathbf{Y} - \mathbf{Y}\mathbf{A}_j\mathbf{X}\mathbf{A}_j^T\mathbf{Y}\right)\mathbf{B}_j\mathbf{B}_j^T \tag{74}$$

so that, the first term in (72) is $\mathbf{B}_j\mathbf{B}_j^T\mathbf{T}_j\mathbf{B}_j\mathbf{B}_j^T = \mathbf{R}_j$.

Each of the remaining three terms in (72) is equal to $\mathbf{0}_{n\times n}$. This can be proved one term at a time by substituting (71) and (73) into these terms, expanding and regrouping to let the term $\mathbf{A}_j^T(\mathbf{I}_n - \mathbf{Y})\mathbf{A}_j\mathbf{X}$ appear. Following definitions of $\mathbf{R}$, $\mathbf{X}$, and $\mathbf{Y}$ in (70), it can be seen that $\mathbf{A}_j^T(\mathbf{I}_n - \mathbf{Y})\mathbf{A}_j\mathbf{X} = \mathbf{A}_j^T\mathbf{A}_j$. This is used to show that the last three terms on the right hand side in (72) cancel out, which concludes the derivation.

APPENDIX D. SS AND CHI-SQUARED RAIM FDE ASSUMING NONZERO MEAN NOMINAL MEASUREMENT ERRORS

The ARAIM implementation in Section VI-D assumes nonzero mean measurement errors, with nominal biases not exceeding $\pm b_{MAX}$. In this case, for SS RAIM FDE, the following four terms, respectively, are the means of the position estimate errors ε_0, ε_i, ε_j, and $\varepsilon_{j,i}$ in the four groups of terms on the right hand side in (36): $\sum_{l=1}^{n}|s_{0,l}|b_{MAX}$, $\sum_{l=1}^{n}|s_{i,l}|b_{MAX}$, $\sum_{l=1}^{n}|s_{j,l}|b_{MAX}$, and $\sum_{l=1}^{n}|s_{ji,l}|b_{MAX}$, where $s_{i,l}$ is the lth element of the $(n-n_i)\times 1$ vector $\mathbf{s}_i$ defined in (20), and $s_{ji,l}$ is the lth element of the $(n-n_i-n_j)\times 1$ vector $\mathbf{s}_{ji}$, which is the LS estimator vector for the state of interest, for the subset solution that excludes both S_i and S_j.

For χ^2 RAIM FDE, the fault vector $\mathbf{f}$ is redefined to incorporate the impact of the nominal measurement biases on faulted measurements $\mathbf{A}_i\mathbf{z}$. Let $\mathbf{b}$ be the $n\times 1$ vector of nominal biases, i.e., the mean of $\mathbf{v}$ in (3). The contributions of $\mathbf{f}$ and $\mathbf{b}$ on $\mathbf{A}_i\mathbf{z}$ are indistinguishable, and can be lumped together. Under H_i, the new fault vector $\mathbf{f}_i$ is defined as

$$\mathbf{f}_i \equiv \mathbf{f} + \mathbf{A}_i\mathbf{A}_i^T\mathbf{b} \tag{75}$$

The impact of $\mathbf{b}$ on the remaining measurements is noted $\mathbf{b}_i$: $\mathbf{b}_i \equiv \mathbf{B}_i\mathbf{B}_i^T\mathbf{b}$. It is worth noting for upcoming derivations that

$$\mathbf{f} + \mathbf{b} = \mathbf{f}_i + \mathbf{b}_i, \quad \mathbf{B}_i\mathbf{B}_i^T\mathbf{f}_i = \mathbf{0}_{n\times 1} \quad \text{and} \quad \mathbf{A}_i\mathbf{A}_i^T\mathbf{b}_i = \mathbf{0}_{n\times 1} \tag{76}$$

First, the means of the estimate errors ε_0 and ε_j in (48) can, respectively, be bounded by $|\mathbf{s}_0^T|\mathbf{B}_i\mathbf{B}_i^T\mathbf{1}_{n\times 1}b_{MAX}$ and $|\mathbf{s}_j^T|\mathbf{B}_i\mathbf{B}_i^T\mathbf{1}_{n\times 1}b_{MAX}$, where $\mathbf{1}_{n\times 1}$ is an $n\times 1$ vector of ones, and the operator $|\bullet|$ designates the element-wise absolute value of the vector argument. Then, the noncentrality parameters of the detection and exclusion test statistics in (48) can be lower-bounded to take into account the worst case impact of $\mathbf{b}$, which maximizes P_{HMI}. Let $\mathbf{D}$ be an $n\times n$ positive semidefinite, symmetric matrix used to generate the test statistic $\mathbf{z}^T\mathbf{D}\mathbf{z}$ ($\mathbf{D} = \mathbf{R}$ for detection, and $\mathbf{D} = \mathbf{T}_j$ for exclusion). Also, let λ^2 designate the noncentrality parameter of this test statistic. λ^2 can be written as

$$\begin{aligned}\lambda^2 &= (\mathbf{f}+\mathbf{b})^T\mathbf{D}(\mathbf{f}+\mathbf{b})\\ &= \mathbf{f}_i^T\mathbf{A}_i\mathbf{A}_i^T\mathbf{D}\mathbf{A}_i\mathbf{A}_i^T\mathbf{f}_i + 2\mathbf{f}_i^T\mathbf{A}_i\mathbf{A}_i^T\mathbf{D}\mathbf{B}_i\mathbf{B}_i^T\mathbf{b}_i\\ &\quad +\mathbf{b}_i^T\mathbf{B}_i\mathbf{B}_i^T\mathbf{D}\mathbf{B}_i\mathbf{B}_i^T\mathbf{b}_i\end{aligned} \tag{77}$$

All terms in (77) are known, except for $\mathbf{b}_i$ whose elements are bounded by $\pm b_{MAX}$. The worst case $\mathbf{f}_i$ can be determined using [19], so that the first of the three terms in (77) is known. Also, since $\mathbf{D}$ is positive semidefinite, the third term is a quadratic form larger than zero. Thus, λ^2 can be lower-bounded using the following expression:

$$\lambda^2 \geq \mathbf{f}_i^T\mathbf{A}_i\mathbf{A}_i^T\mathbf{D}\mathbf{A}_i\mathbf{A}_i^T\mathbf{f}_i - 2\left|\mathbf{f}_i^T\mathbf{A}_i\mathbf{A}_i^T\mathbf{D}\mathbf{B}_i\mathbf{B}_i^T\right|\mathbf{1}_{n\times 1}b_{MAX} \tag{78}$$

where $|\bullet|$ is again the element-wise absolute value of the vector argument. Lower-bounding the noncentrality parameters of q_χ^2 and $q_{\perp,j}^2$ in (48) using (78) provides an upper bound on P_{HMI}. Depending on the value of b_{MAX}, the conservative assumptions made to obtain (78) for χ^2 RAIM may or may not overweight the ones made for SS RAIM in Appendix A.

REFERENCES

[1] Lee, Y. C.
Analysis of range and position comparison methods as a means to provide GPS integrity in the user receiver.
In *Proceedings of the 42nd Annual Meeting of The ION*, Seattle, WA, 1986, 1–4.

[2] Parkinson, B. W., and Axelrad, P.

Autonomous GPS integrity monitoring using the pseudorange residual.
NAVIGATION, **35**, 2 (1988), 225–274.

[3] Sturza, M.
Navigation system integrity monitoring using redundant measurements.
NAVIGATION, **35**, 4 (1988), 69–87.

[4] Brown, R. G.
A baseline GPS RAIM scheme and a note on the equivalence of three RAIM methods.
NAVIGATION, **39**, 3 (1992), 301–316.

[5] Brenner, M.
Integrated GPS/inertial fault detection availability.
NAVIGATION, **43**, 2 (Summer 1996), 111–130.

[6] Blanch, J., Walter, T., and Enge, P.
RAIM with optimal integrity and continuity allocations under multiple failures.
IEEE Transactions on Aerospace and Electronic Systems, **46**, 3 (2010), 1235–1247.

[7] Blanch, J., Walter, T., and Enge, P.
Satellite navigation for aviation in 2025.
Proceedings of the IEEE (special centennial issue), **100** (2012), 1821–1830.

[8] Walter, T., Enge, P., Blanch, J., and Pervan, B.
Worldwide vertical guidance of aircraft based on modernized GPS and new integrity augmentations.
Proceedings of the IEEE, **96**, 12 (2008), 1918–1935.

[9] Blanch, J., Walter, T., Lee, T., Pervan, B., Rippl, M., and Spletter, A.
Advanced RAIM user algorithm description: Integrity support message processing, fault detection, exclusion, and protection level calculation.
In *Proceedings of ION GNSS 2012*, Nashville, TN, Sept. 17-21, 2012, 2828–2849.

[10] Blanch, J., Walter, T., Enge, P., Wallner, S., Fernandez, F. A., Dellago, R., Ioannides, R., Hernandez, I. F., Belabbas, B., Spletter, A., and Rippl, M.
Critical elements for a multi-constellation advanced RAIM.
, *NAVIGATION*, **60**, 1 (Spring 2013), 53–69.

[11] van Graas, F., and Farrell, J.
Baseline fault detection and exclusion algorithm.
In *Proceedings of the 49th Annual Meeting of The ION*, Cambridge, MA, June 1993, 413–420.

[12] Pervan, B., Lawrence, D., Cohen, C., and Parkinson, B.
Parity space methods for autonomous fault detection and exclusion using GPS carrier phase.
In *Proceedings of IEEE PLANS*, Atlanta, GA, 1996.

[13] Joerger, M., and Pervan, B.
Solution separation and chi squared RAIM for fault detection and exclusion.
In *Proceedings of IEEE ION PLANS 2014*, Monterey, CA, May 2014, 294–307.

[14] Vieweg, S.
Integrity monitoring and failure identification within an integrated satellite/inertial navigation system.
In *Proceedings of IEEE PLANS 1994*, 1994, 755—761.

[15] Zhai, Y., Joerger, M., and Pervan, B.
Continuity and availability in dual-frequency multi-constellation ARAIM.
In *Proceedings of ION GNSS 2015*, Tampa, FL, 2015.

[16] International Civil Aviation Organization. Annex 10 to the Convention on International Civil Aviation, Aeronautical Telecommunications, Vol. 1 Radio Navigation Aids, 2006.

[17] EU-US Cooperation on Satellite Navigation, WG C-ARAIM Technical Subgroup. ARAIM Technical Subgroup Milestone 1 Report, 2012. Available online: http://ec.europa.eu/enterprise/newsroom/cf/_getdocument.cfm?doc_id=7793

[18] Wang, J., and Ober, P.
On the availability of fault detection and exclusion in GNSS receiver autonomous integrity monitoring.
The Journal of Navigation of the RIN, **62** (2009).

[19] Joerger, M., Chan, F. C., and Pervan, B.
Solution separation versus residual-based RAIM.
NAVIGATION, **61**, 4 (2014), 273–291.

[20] RTCA Special Committee 159. Minimum aviation system performance standards for the local area augmentation system (LAAS). *RTCA/DO-245*, 2004, Appendix D.

[21] Pullen, S., and Enge, P.
Using outage history to exclude high-risk satellites from GBAS corrections.
NAVIGATION, **60**, 1 (2013), 41–51.

[22] Potter, I. E., and Sunman, M. C.
Threshold-less redundancy management with arrays of skewed instruments.
AGARDOGRAPH - No 224, 1977, 15-11–15-25.

[23] Joerger, M., Stevanovic, S., Chan, F. C., Langel, S., and Pervan, B.
Integrity risk and continuity risk for fault detection and exclusion using solution separation ARAIM.
In *Proceedings of ION GNSS 2013*, Nashville, TN, Sept. 2013, 2702–2722.

[24] Joerger, M., Chan, F. C., Langel, S., and Pervan, B.
RAIM detector and estimator design to minimize the integrity risk.
In *Proceedings of ION GNSS 2012*, Nashville, TN, Sept. 2012, 2785–2807.

[25] Blanch, J., Walter, T., and Enge, P.
Results on the optimal detection statistic for integrity monitoring.
In *Proceedings of ION ITM 2013*, San Diego, CA, Jan. 2013, 262–273.

[26] RTCA Special Committee 159. Minimum Operational Performance Standards for Global Positioning System/Wide Area Augmentation System Airborne Equipment. Document RTCA/DO-229C, Washington, DC, 2001.

[27] Wallner, S., and Boyero, J. P.
Personal conversation within the ARAIM working group C, May 2014.

[28] Almanac files provided by Stanford University. Available online: *http://waas.stanford.edu/staff/maast/maast.html*

[29] Walter, T., and Blanch, J.
Airborne mitigation of constellation wide faults.
In *Proceedings of ION NTM 2015*, Dana Point, CA, Jan. 2015, 676–686.

[30] Meyer, C.D.
Matrix Analysis and Applied Linear Algebra. Philadelphia, PA: Society for Industrial and Applied Mathematics, 2000.

Mathieu Joerger obtained a Master degree in mechatronics from the National Institute of Applied Sciences in Strasbourg, France, in 2002, and an M.S. degree and a Ph.D. degree in mechanical and aerospace engineering from the Illinois Institute of Technology (IIT) in 2002 and 2009, respectively.

He is currently a Research Assistant Professor at IIT, working on multisensor integration, on sequential fault detection for multiconstellation navigation systems, and on relative and differential receiver autonomous integrity monitoring for shipboard landing of military aircraft.

Dr. Joerger was the recipient of the Institute of Navigation (ION) Bradford Parkinson Award (2009), and ION Early Achievement Award (2014).

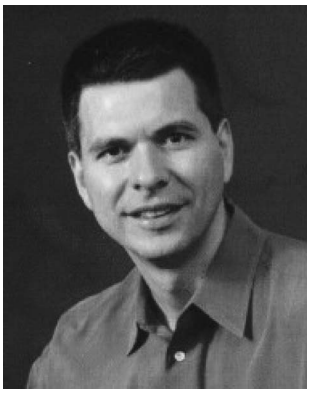

Boris Pervan received his B.S. from the University of Notre Dame, Lafayette, IN, M.S. from the California Institute of Technology, Pasadena, and Ph.D. from Stanford University, Stanford, CA.

He is currently a Professor of Mechanical and Aerospace Engineering at Illinois Institute of Technology (IIT), where he conducts research on advanced navigation systems. Prior to joining the faculty at IIT, he was a spacecraft mission analyst at Hughes Aircraft Company (now Boeing) and a postdoctoral research associate at Stanford University.

Prof. Pervan is an Associate Fellow of the AIAA, a Fellow of the Institute of Navigation (ION), and Editor-in-Chief of the ION journal *NAVIGATION*. He was the recipient of the IIT Sigma Xi Excellence in University Research Award (2011, 2002), Ralph Barnett Mechanical and Aerospace Dept. Outstanding Teaching Award (2009, 2002), Mechanical and Aerospace Dept. Excellence in Research Award (2007), University Excellence in Teaching Award (2005), IEEE Aerospace and Electronic Systems Society M. Barry Carlton Award (1999), RTCA William E. Jackson Award (1996), Guggenheim Fellowship (Caltech 1987), and Albert J. Zahm Prize in Aeronautics (Notre Dame 1986).